Distinguishing among scalar field models of dark energy

Irit Maor* and Ram Brustein†
Department of Physics, Ben-Gurion University, Beer-Sheva 84105, Israel
(Received 18 September 2002; published 21 May 2003)

We show that various scalar field models of dark energy predict a degenerate luminosity distance history of the Universe and thus cannot be distinguished by supernovae measurements alone. In particular, models with a vanishing cosmological constant (the value of the potential at its minimum) are degenerate with models with a positive or negative cosmological constant whose magnitude can be as large as the critical density. Adding information from CMB anisotropy measurements does reduce the degeneracy somewhat but not significantly. Our results indicate that a theoretical prior on the preferred form of the potential and the field's initial conditions may allow one to quantitatively estimate model parameters from the data. Without such a theoretical prior only limited qualitative information on the form and parameters of the potential can be extracted, even from very accurate data.

DOI: 10.1103/PhysRevD.67.103508 PACS number(s): 98.80.Cq, 98.80.Es

I. INTRODUCTION

One of the standard methods of interpreting the growing body of evidence from supernovae [1] and other measurements that the expansion of the Universe is accelerating is to assume the existence of a dark energy component and to model it using scalar fields (for a recent review see Ref. [2]). This links the expansion history of the Universe to theories of fundamental physics. For example, from this perspective the value of the potential at its minimum is the cosmological constant (CC). Since at this point there are many theoretical ideas about the form of the potential but none that particularly stands out, it would have been helpful if the data from cosmological measurements, such as supernovae type Ia, cosmic microwave background (CMB) and various others, could provide hints about some generic features of the potential.

Viable scalar field models of dark energy need to have potentials whose energy scale is about the critical density $\sim 10^{-12}$ eV^4, and typical scalar field masses about the Hubble mass $m \sim 10^{-33}$ eV. In such models typical scalar field variations are about the Planck scale $m_p \sim 10^{19}$ GeV, and typical time scales for such variations are about the Hubble time $1/H_0 \sim 10^{18}$ sec. Whether, and how well, it is possible to determine the parameters and form of the potentials and the field's dynamical history and future from data beyond such qualitative estimates has been addressed previously [3–11]. Weller and Albrecht [5] concluded that some potentials could be differentiated using SNAP-like data [12]. They approximated the equation of state (EOS) of each of the models, and showed by likelihood analysis that some of the models are distinguishable. Another approach is ''reconstruction'' [9–11]. Here one rewrites the potential as a function of the luminosity distance (d_L) and its derivatives, which are in turn functions of the redshift. The potential (and not the EOS) is approximated by a fitting function, and statistically tested against a set of accurate d_L measurements. The efficiency of reconstruction depends on the accuracy of knowing the values of Ω_m (this is needed also when one fits the EOS) and H_0 (this is needed only for reconstruction). On general grounds we expect that scalar field potentials are less distinguishable than their corresponding EOS, because different potentials, with properly adjusted initial conditions for the field can produce a very similar EOS.

In previous papers [13,14] we have found that supernovae (SN) measurements are limited as a probe of the dark energy EOS w_Q, due to degeneracies. Specifically, it was shown that d_L's corresponding to two different w_Q's are degenerate if both EOS coincide at some point at a relatively low redshift, z^* (see also Refs. [15] and [16]). The purpose of the present analysis is to explore the implications of this degeneracy on the possibility to determine the scalar field potential. For a given functional form of potential, we would like to quantify the amount by which the parameters of the potential can be varied, and still be indistinguishable by accurate SN measurements. Our criteria for indistinguishability between two models is that their resulting d_L's differ at most by 1% up to redshift $z=2$, in accordance with the anticipated accuracy of future SN measurements. In addition, we would like to determine whether the functional form of the potential can be distinguished or constrained by data.

We look for degeneracies among potentials using the following procedure: For a given class of potentials, we change the parameters as well as the initial values of the field, with the constraint that w_Q at z^* remains unchanged. This results in models whose w_Q cross at z^*. We know from our previous analysis that in this case the models tend to be degenerate. Then we evaluate numerically the differences in the d_L's of the models to verify this.

There are additional sources of degeneracy that we do not consider here. In our procedure the value of the potential energy and the value of the kinetic energy remain unchanged. Allowing changes in the potential that are compensated by changes in the initial conditions for the kinetic energy will give another dimension of degeneracy. Variation in the value of Ω_m is yet another degree of freedom, as is relaxing the assumption of a flat Universe and considering the effects of a clumpy Universe [17]. Additionally, the value of

*Email address: irrit@bsumail.bgu.ac.il
†Email address: ramyb@bgumail.bgu.ac.il

z^* in different models can be shifted. We have found that z^* varies slowly with the redshift depth of the data set $z_{\max}$. The dependence is approximately linear $z^*=\alpha z_{\max}+\beta$ (see also Ref. [18]), α and β are model dependent but α is typically small, about 0.2. And, finally, we have looked only at a class of simple potentials that have two independent parameters. Additional parameters in the potential yet again open up new degrees of freedom, each of which increases the degeneracy of each of the parameters. Since we have found that this class of simple potentials suffers from large degeneracies, we see no phenomenological justification for using more complex potentials. If a theoretical prior about the form of the potential and initial conditions can be motivated then some of this degeneracy can be removed.

II. DEGENERACIES OF SCALAR FIELD POTENTIALS

We consider a flat Universe with nonrelativistic matter (dark matter included) whose EOS is $w_m=0$, and a dark energy component which we model by a canonically normalized and minimally coupled scalar field. Einstein's equations for such a universe are the following:

$$H^2=\kappa^2\left(\rho_m x^3+\frac{1}{2}x^2H^2\phi'^2+V(\phi)\right) \tag{1}$$

$$xHH'=\frac{3\kappa^2}{2}(\rho_m x^3+x^2H^2\phi'^2) \tag{2}$$

$$x^2H^2\phi''+(x^2HH'-2xH^2)\phi'+\frac{dV}{d\phi}=0, \tag{3}$$

where $x=1+z$, $\kappa^2=8\pi/3m_p^2$, ρ_m is the matter energy density today, primes denote derivatives with respect to x, and V is the potential of the scalar field. The scalar field's EOS (w_Q) is given by

$$w_Q=\frac{p_Q}{\rho_Q}=\frac{x^2H^2\phi'^2-2V}{x^2H^2\phi'^2+2V}. \tag{4}$$

We choose a model, and vary the parameters of the potential P_i, as well as the values of the scalar field at z^* keeping its derivative constant:

$$\phi(z^*)\to\phi(z^*)+\delta\phi, \tag{5}$$

$$V\to V+\delta V(P_i,\delta P_i,\delta\phi), \tag{6}$$

$$\delta\phi'(z^*)=\delta H(z^*)=\delta\rho_m=0. \tag{7}$$

These variations result in variations in Eqs. (4) and (1):

$$w_Q+\delta w_Q=\frac{x^2H^2\phi'^2-2(V+\delta V)}{x^2H^2\phi'^2+2(V+\delta V)}\approx w_Q+\left[\frac{2(1+w_Q)}{x^2H^2\phi'^2+2V}\right]\delta V+\mathcal{O}(\delta V^2) \tag{8}$$

$$H^2=\kappa^2\left(\rho_m x^3+\frac{1}{2}x^2H^2\phi'^2+(V(\phi)+\delta V)\right). \tag{9}$$

In Eq. (8), we have kept terms up to first order in δV, assuming it is small enough.

Since we know that if the values of $w_Q(z^*)$ are equal for two models then their luminosity-distance history is approximately degenerate, we explore part of the degeneracy in parameter space by requiring that $\delta w_Q(z^*)$ vanishes. In Eq. (8) we ignore higher orders in δV, so we simply require that δV vanishes to first order. On the other hand, even a small deviation from a spatially flat cosmology will be amplified by the evolution of the solution. We therefore need to require that Eq. (9) holds exactly.

The two constraints we are imposing are then

$$\delta V(P_i,\delta P_i,\delta\phi)^{(1)}=0, \tag{10}$$

$$\delta V(P_i,\delta P_i,\delta\phi)^{(\text{exact})}=0. \tag{11}$$

This set of variations and constraints is algebraic and can often be solved analytically. The analytical solution connects any given model to a family of associated models, all of which have the same w_Q at z^*. The next step is to check numerically how large are the allowed parameter variations such that different models in the family are indistinguishable [25].

Initial conditions are given at z^*, but the evolution of each of the models towards $z=0$ is different, and they end up with a different value of H_0 (Hubble parameter at $x=1$, $z=0$). To ensure that all models have the same value of H_0 we rescale them:

$$\tilde{H}=\frac{H}{H_0},\quad \Omega_m=\frac{\rho}{H_0^2m_p^2},\quad \tilde{\phi}=\frac{\phi}{m_p},\quad \tilde{V}=\frac{V}{H_0^2m_p^2}. \tag{12}$$

Equation (1) can be reexpressed in terms of the rescaled variables

$$\tilde{H}^2=\Omega_m x^3+\frac{1}{2}x^2\tilde{H}^2\tilde{\phi}'^2+\tilde{V}. \tag{13}$$

This means that although initially only the scalar field potential energy is varied, eventually all quantities (except H_0) may vary between models. As we shall show later (Sec. III), it turns out that differences in Ω_m are negligible. This result is not surprising: as was shown in [14] (see in particular Fig. 2), this type of degeneracy characterizes models with fixed values of Ω_m. Families of models which are degenerate with respect to SN measurements but have different values of Ω_m

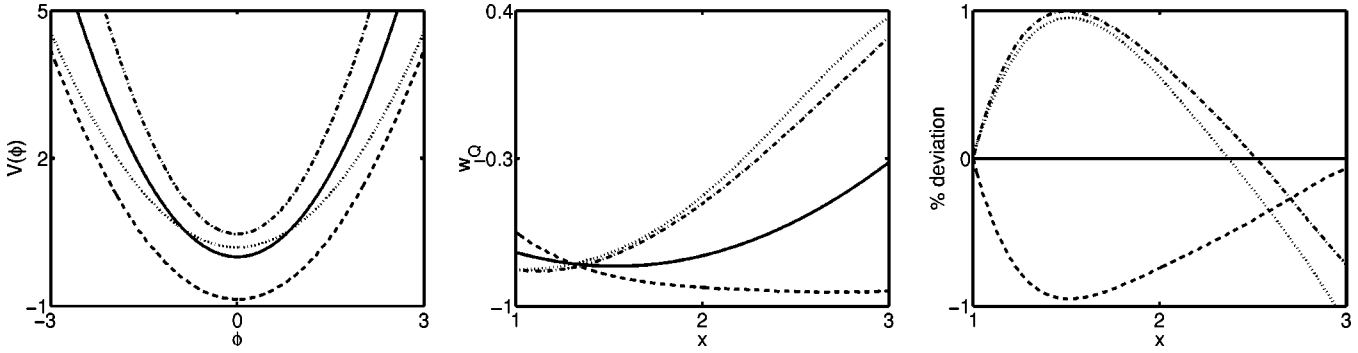

FIG. 1. Various quadratic potentials (shown on the left), their resulting w_Q (middle), and the relative difference in d_L (right). The parameters of the potentials are listed in Table I.

do not exhibit the enhanced resolution of $w_Q(z^*)$. This means that on top of the degeneracy that we will be exploring here, another dimension of degeneracy will open up once the uncertainties in Ω_m are taken into account. The method described here therefore exposes only part of the degeneracy among potentials.

III. DEGENERACIES AMONG SIMPLE POTENTIALS

We have analyzed various forms of potentials with two parameters. For all such potentials there are three independent variations, two parameters and the initial condition for ϕ. Enforcing the two constraints (10),(11) results in a solution which is a curve in a three-dimensional space. Obviously the degeneracy is larger when more parameters are allowed.

One class of potentials we have looked at is $V(\phi) = \frac{1}{2}m^2\phi^2 + v_0$. This is one of the standard simple forms of potentials, m is the scalar field mass, v_0 is the value of the potential at the minimum (the CC). As explained previously we already have an order of magnitude estimates for v_0 and m, but we would like to know whether they can be determined in a more quantitative and conclusive way by the data. In particular we would like to know whether it is possible to distinguish models with a vanishing CC ($v_0 = 0$) from models with a nonvanishing CC ($v_0 \neq 0$) [26]. For this class of quadratic potentials the variation is given by

$$\begin{aligned} V + \delta V &= \frac{1}{2}(m+\delta m)^2(\phi+\delta\phi)^2 + (v_0+\delta v_0) \\ &= \left[\frac{1}{2}m^2\phi^2 + v_0\right] + [m^2\phi\,\delta\phi + m\phi^2\delta m + \delta v_0] \\ &\quad + \left[\frac{1}{2}(m\,\delta\phi + \phi\,\delta m)^2 + \delta\phi\,\delta m(m+\delta m)(\phi+\delta\phi)\right. \\ &\quad \left. - \frac{1}{2}\delta m^2\,\delta\phi^2\right]. \end{aligned} \tag{14}$$

The first bracket is V itself. The second bracket is $\delta V^{(1)}$ which should vanish, and the last bracket is $\delta V^{(\mathrm{exact})} - \delta V^{(1)}$ which should vanish as well. The solution is a curve in the $(\delta v_0,\ \delta m,\ \delta\phi)$ space. On this curve changes in the curvature and the height of the minimum of the potential are compensated by a change in the value of ϕ such that the potential energy of the field is locally unchanged.

Figure 1 shows a variety of quadratic potentials on the left, their resulting w_Q in the middle, and the relative difference in d_L on the right. The parameters of the potentials are listed in Table I. Notice that although the fiducial model has a vanishing CC, $v_0 = 0$, it is degenerate with models that have v_0 of order unity in units of the critical density $(m_p^2 H_0^2)$. The uncertainty in m is of order unity in units of the present value of the Hubble parameter H_0.

All the models have values of Ω_m which are within ± 0.01 from the value of the fiducial. This means that we are indeed exploring here the degeneracy due to the integral relation between d_L and w_Q, and not the degeneracy due to the uncertainty in Ω_m. As explained previously, this is a direct consequence of our method.

Following the same procedure we have analyzed other popular classes of potentials with two parameters. Figure 2 shows similar results for an exponential potential $V = Ae^{-B\phi}$. For this specific potential only some of the solutions of Eqs. (10) and (11) can be found analytically, hence the degeneracy shown is a smaller than the full degeneracy, as can be seen by the reduced range of allowed values of A in Table II. Figure 3 shows the results for an inverted quadratic potential $V = -\frac{1}{2}m^2\phi^2 + v_0$ (also see Table III).

As can be seen from the figures, the deviation in d_L tends to peak at low redshift, about $z = 0.4$. This results from the following reason: consider two models whose EOS cross at $z = z^*$. For redshifts $z < z^*$, the different w_Q of the models imply different rates of expansion. The model whose w_Q is more negative will expand faster, making the d_L's of the two models diverge. In the range $z > z^*$ the trends reverse, making their d_L's converge. If this were the only source of degeneracy among models, it would have been useful to focus

TABLE I. Parameters of quadratic potential plotted in Fig. 1.

	Solid (fiducial)	Dashed	Dotted	Dash-dotted
$(m/H_0)^2$	1.51	1.12	0.98	1.99
$v_0/m_p^2H_0^2$	0	−0.86	0.20	0.47
Ω_m	0.30	0.31	0.29	0.29

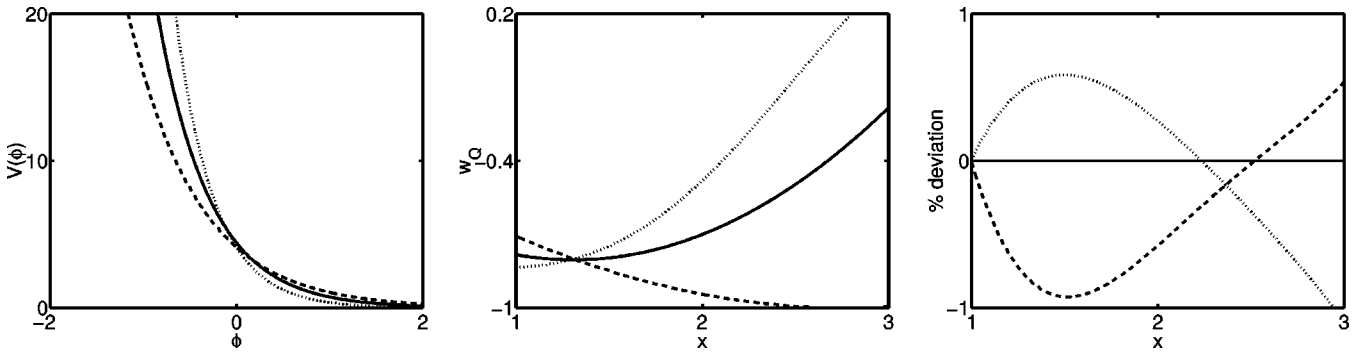

FIG. 2. Various exponential potentials (shown on the left), their resulting w_Q (middle), and the relative difference in d_L (right). The parameters of the potentials are listed in Table II.

measurements in this range of redshifts $z\sim0.4$. Unfortunately a second degeneracy (due to the uncertainty in Ω_m) degrades the extra sensitivity in this region of redshifts.

So far we have analyzed the uncertainty in determination of parameters under the assumption that the form of the potential is known. Without a theoretical prior on the form of the ''true'' potential it is important to find whether different classes of potentials can be distinguished by the data alone. We will present here only a representative example and not attempt a systematic analysis to expose the full degeneracy.

In Fig. 4 we show an example of four different degenerate potentials. All models have $\Omega_m=0.30$. The potentials we have used in this example are $V=\frac{1}{2}m^2\phi^2+v_0$ (solid), $V=Ae^{-B\phi}$ (dotted), $V=-\frac{1}{2}m^2\phi^2+v_0$ (dashed), and $V=a+b\phi$ (dash dotted). The right panel shows that the relative differences in their d_L's are less than one percent up to $z=2$. The left panel shows the potentials. Although the functional forms of the potentials are very different and they do not have the same asymptotic behavior, they are nevertheless indistinguishable. This can be understood by observing that the patch of potential that was probed by the field during the relevant redshift range (marked in the figure by the shaded area) is rather small. In this patch, differences among the various potentials are marginal.

The fact that a small patch of the potential is actually being probed justifies the use of a simple potential with a small number of parameters. A fast rolling field would have served as a better probe of the potential since it would have covered a larger patch in a given redshift range, but this would have meant a more positive w_Q which goes against the evidence of accelerated expansion. Another possible way to enlarge the size of the probed potential patch would have been to measure d_L over a larger redshift range. The difficulty here is that at deeper redshifts the contribution of dark energy to the total energy of the Universe is smaller, and its effects become harder to detect.

TABLE II. Parameters of exponential potential plotted in Fig. 2.

	Solid (fiducial)	Dashed	Dotted
$A/m_p^2H_0^2$	4.43	4.13	4.12
m_pB	1.78	2.40	1.36
Ω_m	0.30	0.30	0.29

Our results may seem to disagree with those of Ref. [5], where it was shown that different forms of potentials could be distinguished using SNAP-like data alone, but we believe that they are in fact in full agreement. Our interpretation of the results of Ref. [5] is that they depend on the choice of specific parameters and initial conditions for each of the potentials that makes them distinguishable. This does not mean that for a given set of data, it will be possible to determine that a specific class of potentials is preferred over another. It is quite easy to construct counter examples by choosing the potentials to look similar in the relevant redshift patch. A representative example is shown in Fig. 5. The potentials that are used here are the pseudo Nambu-Goldstone boson potential $V=M^4[\cos(\phi/f)+1]$ [with $M^4/(m_p^2H_0^2)=0.82$ and $f/m_p=0.6$] and the pure exponential $V=Ae^{-B\phi}$ [with $A/(m_p^2H_0^2)=4.43$ and $m_pB=1.78$].

IV. CONSIDERING CMB

An additional measurement that can possibly probe the dark energy EOS and the scalar field potential is that of the cosmic microwave background (CMB) anisotropy. This measurement is expected to be improved with the upcoming Microwave Anisotropy Probe (MAP) and Planck missions.

We would like to show that under reasonable assumptions, CMB measurements will not help to significantly constrain the scalar field potential. The key reason is that the CMB can be thought of as providing one additional point on the Hubble diagram, with sensitivity that does not add significant resolving power compared to accurate measurements at lower redshifts. This can be motivated by a semianalytical argument that we present at the end of this section.

Using the CMB measurements to probe scalar field models requires additional theoretical assumptions about the evolution in the range from $z\sim2$ to $z\sim1000$ to impose the obvious constraint that the dark energy had negligible influence on the geometry and expansion history of the universe above a redshift of a few (say, $z=2$). For example, that the potentials are ''tracker'' potentials [19].

Scalar field models that are not chosen as tracker models, such as the toy models that we have used in the previous sections, will give result that are in blatant contradiction with observations. If the equations of motion are allowed to evolve backwards from $z\sim0.3$ up to $z\sim1000$ without any

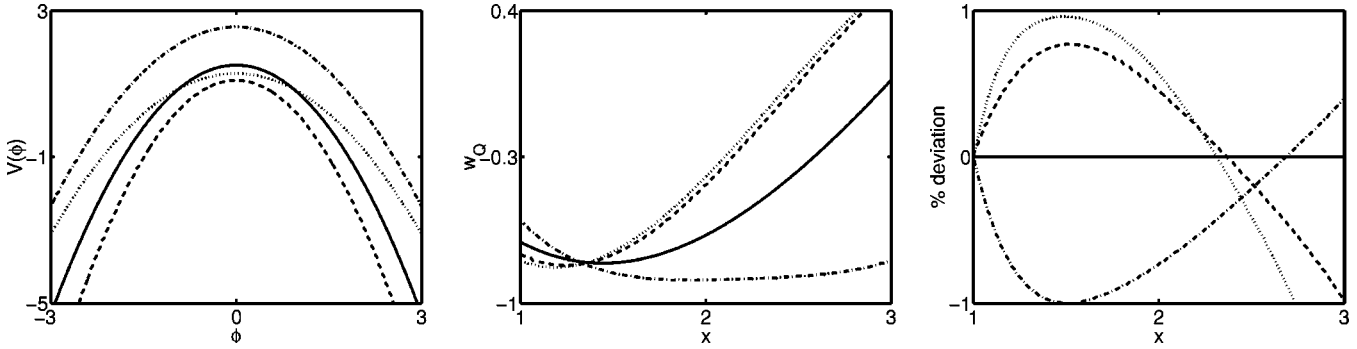

FIG. 3. Various inverted quadratic potentials (shown on the left), their resulting w_Q (middle), and the relative difference in d_L (right). The parameters of the potentials are listed in Table III.

changes, the dark energy typically becomes dominant, with w_Q approaching 1. In order to to avoid such undesirable and observationally excluded behavior, the class of models needs to be enlarged and more parameters need to be added to accommodate the requirement that the effect of the scalar field component should have been negligible in the past. For example, considering an inverted quadratic potential, one needs to allow for a quartic term such that a minimum with zero CC is available.

Instead of modifying the potential, we have chosen another approach that mimics the essential feature of any acceptable class of models: that the scalar field effects are subdominant until recently, when they do become the dominant energy component and reveal their dynamical nature. In the spirit of Ref. [14] we let the equations of motion evolve until $z=2$ (the redshift range relevant to SN measurement), and for $z>2$ we change the EOS (and not the potential) by setting $w_f \equiv w_Q(z>2)=-1$ for all models. We then calculate numerically the relative differences in d_L at $z=1000$. This approach is technically much simpler to implement and study and has the advantage that the results are transparent. One expects that the details of the changes to the EOS (cutoff) be unimportant, since this is done at a redshift when the dark energy density is already negligible.

We have checked whether the results depend on the particular way in which the EOS cutoff is implemented in several ways and found, as expected, that for many cutoff procedures the results are quite robust. For example, we have checked which value for w_f is the least sensitive to the cutoff details. We have found that there is essentially no sensitivity for $w_f=-1$, and the sensitivity grows as the value of w_f becomes less negative. For $w_f=0$, the cutoff details become important. As an example, comparing two cutoffs for the mass potential from Fig. 4 gives a relative difference of 0% for $w_f=-1$, 0.2% for $w_f=-0.7$, and 13% for $w_f=0$.

TABLE III. Parameters of inverted quadratic potentials plotted in Fig. 3.

	Solid (fiducial)	Dashed	Dotted	Dash-dotted
$(m/H_0)^2$	1.51	1.88	0.98	1.08
$v_0/m_p^2 H_0^2$	1.51	1.09	1.28	2.55
Ω_m	0.30	0.29	0.29	0.31

These results are reasonable because the dark energy component effectively disappears for $w_f<0$, while for $w_f=0$ any tampering with it is imprinted all the way to last scattering surface.

It is well known that the EOS cannot be determined using CMB anisotropy data alone due to degeneracies. A thorough analysis was done in Ref. [20], who concluded that this degeneracy persists after combining CMB and SN measurements. In Ref. [14] it was shown that the inclusion of CMB constraints in the analysis of the dark energy EOS does improve the resolution somewhat, but not significantly.

In a simple minded estimate here, we would like to show that under reasonable assumptions, CMB measurements will not help to significantly constrain the potential either. Rather than performing an extensive numerical search, as in Refs. [14,21], we use a different strategy: we treat CMB measurements as effectively providing one additional point on the Hubble diagram at the last scattering redshift $z_{ls}\sim 1000$ as done also in Ref. [22]. The method cannot provide numerically accurate results, but it does highlight the theoretical degeneracy that limits the ability of CMB measurements to constrain the parameters and functional form of the potential.

Treating the CMB measurements as effectively one additional point on the Hubble diagram at redshift $z\sim 1000$ can be implemented in a simple way because the angular distance and the luminosity distance are related to each other $d_L=(1+z)^2 d_A$. The observed angular size of any feature in the CMB θ is related to its physical size d by the angular distance d_A to last scattering surface $\theta d_A = d$. The CMB spectrum yields a series of acoustic peaks, located at $l_n = (n\pi/S) d_A$, n being an integer, and S is the sound horizon at last scattering surface. We are going to ignore uncertainties in the sound horizon S, which depends on the composition of the universe at last scattering surface. Additionally, the value of H_0 (or h) is similar in all our models, by construction.

To estimate the measurement accuracy of the CMB point on the Hubble diagram we may treat the position of the first peak l_1, as a direct measurement of the angular distance, therefore the relative errors in l_1 and in the angular distance are equal $\Delta l_1/l_1 = \Delta d_A/d_A$. The position of the first peak is already measured rather well, to about 3% at the 1σ level (see, for example, Ref. [23]). A recent analysis of fitting CMB peaks with Gaussians [24] gives similar results. This is

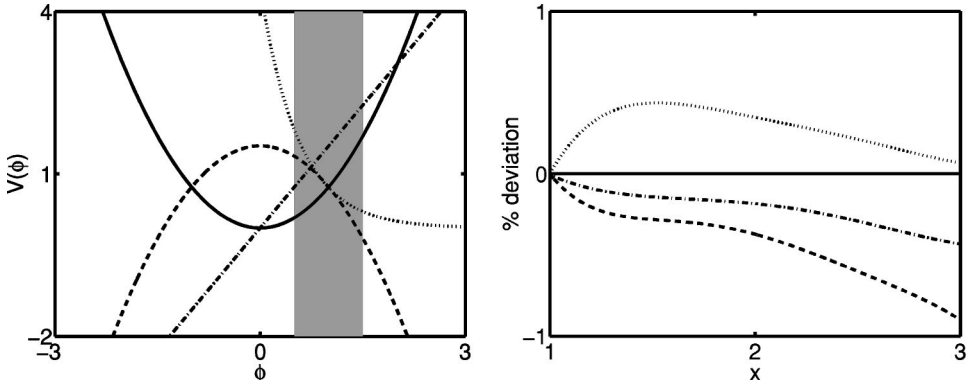

FIG. 4. Various potentials (left panel) and their relative d_L differences (right panel). The potentials we have used in this example are $\frac{1}{2}m^2\phi^2+v_0$ (solid), $Ae^{-B\phi}$ (dotted), $-\frac{1}{2}m^2\phi^2+v_0$ (dashed), and $a+b\phi$ (dash dotted). All models have $\Omega_m=0.30$. The shaded area in the figure on the left indicates the region in which the field moves in the relevant redshift range $0\leqslant z\leqslant 2$.

expected to be somewhat improved by MAP and Planck, so we may expect eventually a 1σ error in the subpercent range.

Another way of estimating the accuracy of the CMB point is to use the results of Ref. [14], where it was shown that for models which have a linear w_Q for $z<2$ and $w_Q=$const from $z=2$ to last scattering surface, a derivative as large as $w_1=\pm\frac{1}{6}$ could not be distinguished at the 3σ level, assuming full sky coverage and cosmic variance limited measurement. This means that the most accurate CMB measurements do not distinguish models which lead to a difference of $(+1.6\%, -3.2\%)$ in their d_L's. Thus a 1σ measurement error estimate in d_L in the subpercent range seems reasonable.

According to the preceding discussion we may define models to be indistinguishable by the CMB if their d_L difference is less than a few percent at z_{ls}. We may check now whether this imposes additional constraints on our models. We find that it does, but not to a significant degree.

We find that the relative differences in d_L for our models are within a few percent, in agreement with the semianalytic argument that we present shortly. For the potentials shown in Fig. 4, we find $\Delta d_L/d_L=0\%$ for the exponential potential, -0.4% for the inverted quadratic potential, and -0.2% for the linear potential. For the quadratic potential examples in Fig. 1 we find the following d_L differences from the fiducial, dashed: 0%, dot-dashed: -0.3%, dotted: -0.4%, for the exponential potentials of Fig. 2 we find dashed: 0.3%, dotted: -0.5%, and for the inverted quadratic potential of Fig. 3 we find dashed: -0.4%, dotted: -0.4%, and dot-dashed: 0.2%. As explained previously this is roughly at the limit of the CMB resolution.

For most of the models we see that CMB is expected to further constrain the parameters if the form of the potential is known. In general, the larger d_L differences are for models whose differences at $z\sim 2$ are larger, in agreement with the following semianalytic argument. Given the approximate nature of our measurement accuracy estimate, the large number of additional sources of degeneracy that we have neglected, and the additional theoretical assumptions that go into the analysis with the CMB point added it is not possible, and we believe that it is not necessary to determine in a more quantitative way the amount by which the degeneracy is reduced.

We may estimate in a rough semianalytic way the relative errors in d_L at $z\sim 1000$ as follows. Luminosity distance at $1+z_{ls}=x_{ls}\approx 1000$ for models with negligible $\Omega_Q(x>3)$ is given by [14]

$$
\begin{aligned}
d_L(x_{ls}) &= x_{ls}\int_1^{x_{ls}}\frac{dx}{H(x)} \\
&= x_{ls}\int_1^{3}\frac{dx}{H(x)}+x_{ls}\int_3^{x_{ls}}\frac{dx}{H(x)} \\
&= \frac{x_{ls}}{3}d_L(3)+\frac{x_{ls}}{H(3)}\int_3^{x_{ls}}\frac{dx}{H(x)/H(3)} \\
&= \frac{x_{ls}}{3}d_L(3)+\frac{x_{ls}}{H(3)}\int_3^{x_{ls}}\frac{dx}{(x/3)^{3/2}} \\
&= \frac{x_{ls}}{3}d_L(3)+2x_{ls}\left(\frac{1}{\sqrt{3}}-\frac{1}{\sqrt{x_{ls}}}\right)\left(\frac{3^{3/2}}{H(3)}\right), \qquad (15)
\end{aligned}
$$

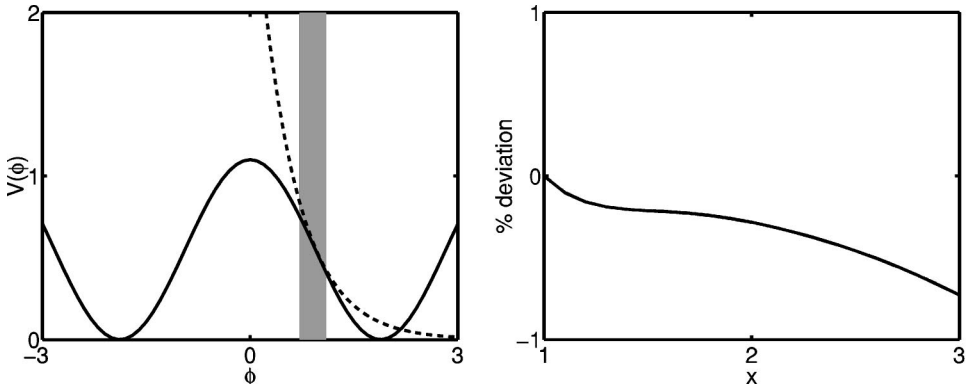

FIG. 5. Two potentials (shown on the left), and their relative d_L differences (right). The potentials we have used in this example are $v=M^4[\cos(\phi/f)+1]$ (solid) and $Ae^{-B\phi}$ (dashed). Both models have $\Omega_m=0.30$. The shaded area in the left panel indicates the region in which the field moves in the relevant redshift range $0\leqslant z\leqslant 2$.

where we have set H_0 to unity, and used $H(x)/H(3) = (x/3)^{3/2}$ because $\Omega_Q(x>3)$ is negligible.

The second term can be expressed in terms of the luminosity distance at $x=3$ and its derivative

$$\frac{1}{H(3)} = \frac{d}{dx}\left(\frac{d_L}{x}\right)_{x=3} \tag{16}$$

so

$$d_L(x_{ls}) \simeq -\frac{x_{ls}}{3} d_L(3) + 2x_{ls} d_L'(3). \tag{17}$$

Now we would like to examine the difference in $d_L(x_{ls})$ for two models. For a simple and rough error estimate, we may use $d_L'(3) = c_1[d_L(3)/3]$ and $\Delta d_L'(3) = c_2[\Delta d_L(3)/3]$ with c_1, c_2 numerical coefficients of order unity. So finally we obtain

$$\left(\frac{\Delta d_L}{d_L}\right)_{x_{ls}} \simeq \frac{2c_2 - 1}{2c_1 - 1}\left(\frac{\Delta d_L}{d_L}\right)_{x=3}. \tag{18}$$

Note that the relative d_L error at x_{ls} is independent of x_{ls}. Since we consider models whose maximal relative error at $z=2$ is one percent, they will have a relative error in d_L of about a few percent at z_{ls}, depending on the values of c_1 and c_2. This estimate agrees with the numerical examples that we have listed above.

We conclude that once physically reasonable constraints are imposed on the potential, CMB measurements do not significantly constrain the parameter space of the potentials, although they are expected to reduce it somewhat. Our simple minded analysis strengthens the case first made in Ref. [20] where it was shown that only some average EOS can be measured, and agrees with Refs. [18,22].

V. CONCLUSIONS

We have found that it is not possible to obtain precise quantitative estimates for parameters of scalar field models of dark energy from data alone beyond the obvious order of magnitude estimates. This is due to theoretical degeneracies, which would persist even with expected future data from the most accurate SN and CMB measurements.

Theoretical prior knowledge or assumptions on the form of the potential and the field's initial conditions (preferably leaving a total of just two free parameters) may allow a more quantitative determination. For example, assuming that the field is at rest at the bottom of the potential is equivalent to having a pure cosmological constant. In this case the magnitude of the cosmological constant can be determined with accurate data to within a few percent.

ACKNOWLEDGMENTS

We wish to thank Sarah Bridle, Rob Critteden, and Carolina Odman for helpful discussions. I.M. gratefully acknowledges support from the Clore foundation.

[1] Supernova Cosmology Project Collaboration, S. Perlmutter *et al.*, Astrophys. J. **517**, 565 (1999); B. P. Schmidt *et al.*, *ibid.* **507**, 46 (1998); Supernova Search Team Collaboration, A. G. Riess *et al.*, Astron. J. **116**, 1009 (1998).
[2] P. J. Peebles and B. Ratra, "The cosmological constant and dark energy," astro-ph/0207347.
[3] T. Chiba and T. Nakamura, Phys. Rev. D **62**, 121301(R) (2000).
[4] V. D. Barger and D. Marfatia, Phys. Lett. B **498**, 67 (2001).
[5] J. Weller and A. Albrecht, Phys. Rev. D **65**, 103512 (2002).
[6] S. C. Ng and D. L. Wiltshire, Phys. Rev. D **64**, 123519 (2001).
[7] S. A. Bludman and M. Roos, Phys. Rev. D **65**, 043503 (2002).
[8] M. Eriksson and R. Amanullah, Phys. Rev. D **66**, 023530 (2002).
[9] D. Huterer and M. S. Turner, Phys. Rev. D **60**, 081301 (1999).
[10] T. D. Saini, S. Raychaudhury, V. Sahni, and A. A. Starobinsky, Phys. Rev. Lett. **85**, 1162 (2000).
[11] B. F. Gerke and G. Efstathiou, Mon. Not. R. Astron. Soc. **335**, 33 (2002).
[12] http://snap.lbl.gov/
[13] I. Maor, R. Brustein, and P. J. Steinhardt, Phys. Rev. Lett. **86**, 6 (2001); **87**, 049901(E) (2001).
[14] I. Maor, R. Brustein, J. McMahon, and P. J. Steinhardt, Phys. Rev. D **65**, 123003 (2002).
[15] D. Huterer and M. S. Turner, Phys. Rev. D **64**, 123527 (2001).
[16] P. Astier, "Can luminosity distance measurements probe the equation of state of dark energy," astro-ph/0008306; M. Goliath, R. Amanullah, P. Astier, A. Goobar, and R. Pain, "Supernovae and the nature of the dark energy," astro-ph/0104009.
[17] D. Munshi and Y. Wang, Astrophys. J. **583**, 566 (2003); M. Sereno, E. Piedipalumbo, and M. V. Sazhin, Mon. Not. R. Astron. Soc. **335**, 1001 (2002).
[18] E. V. Linder and D. Huterer, Phys. Rev. D **67**, 081303(R) (2003).
[19] I. Zlatev and P. J. Steinhardt, Phys. Lett. B **459**, 570 (1999).
[20] G. Huey, L. M. Wang, R. Dave, R. R. Caldwell, and P. J. Steinhardt, Phys. Rev. D **59**, 063005 (1999).
[21] P. S. Corasaniti and E. J. Copeland, Phys. Rev. D **65**, 043004 (2002).
[22] J. A. Frieman, D. Huterer, E. V. Linder, and M. S. Turner, Phys. Rev. D **67**, 083505 (2003).
[23] W. Hu and S. Dodelson, "Cosmic Microwave Background Anisotropies," astro-ph/0110414; C. J. Odman, A. Melchiorri, M. P. Hobson, and A. N. Lasenby, Phys. Rev. D **67**, 083511 (2003).
[24] K. Grainge *et al.*, "The CMB power spectrum out to l=1400 measured by the VSA," astro-ph/0212495.
[25] Recall that our criterion for indistinguishable models is that their d_L's do not differ by more than 1% in the range $0 \leqslant z \leqslant 2$.
[26] It is worth noting here that although $v_0 \neq 0$ is interpreted as a contribution to the vacuum energy which has $w_\Lambda = -1$, offsetting v_0 from zero and allowing V to have negative regions can yield $|w_Q| > 1$ while the field is still dynamical. For example, if $V = -KE/3$ (KE is the kinetic energy of the field), then $w_Q = (KE - V)/(KE + V) = 2$.